Stabilization of BH_4 Group in Zinc Borohydride via Adduct of Ammonia towards a Pure Hydrogen Release

Liang Gao,[a] Yanhui Guo,[a] Kia Wallwork,[b] Feiwu Zhang,[c] Xuebin Yu*[a]

$Zn(BH_4)_2 \cdot 2NH_3$, a new ammine metal borohydride, has been synthesized via simply ball-milling a mixture of $ZnCl_2 \cdot 2NH_3/2LiBH_4$. Structure analysis shows that the subsequent complex has a monoclinic structure with unit-cell parameters of a = 6.392(4) Å, b = 8.417(6) Å, c = 6.388(4) Å and β = 92.407(4) ° and space group $P2_1$, in which Zn atoms coordinate with two BH_4 groups and two NH_3 groups. The interatomic distances reported herein show that Zn-H bonding in $Zn(BH_4)_2 \cdot 2NH_3$ is shorter than Ca-H bonds in $Ca(BH_4)_2 \cdot 2NH_3$ and Mg-H in $Mg(BH_4)_2 \cdot 2NH_3$. This reduced bond contact leads to an increase in the ionic character of H. This study is able to show a good correlation between the reduced M-H distance and enhanced dehydrogenation behavior of the hydride material. Dehydrogenation results showed that this novel compound is able to release 8.9 wt. % hydrogen below 115 °C within 10 min without concomitant release of undesirable gases such as ammonia and/or boranes, thereby demonstrating the potential of $Zn(BH_4)_2 \cdot 2NH_3$ to be used as a solid hydrogen storage material.

Introduction

Hydrogen is considered one of the environmentally clean energy carriers, as it achieves nearly zero emission of pollutants from power generators, such as fuel cells. However, efforts to make use of hydrogen as an on-board power source have been hampered by the safety concerns and volumetric constraints.[1-4] In order for the wide-spread, practical use of hydrogen as an energy provider, it is necessary to store the gas in such a way as to achieve a high energy density, in addition it is important for storage materials to be easily produced and subsequently used. Meeting these criteria will allow the efficient use of hydrogen storage materials. There is no doubt that if the hydrogen economy is to meet the practical application requirements then fundamental and applied research must provide the breakthrough in identifying and understanding hydrogen-rich materials.[5,6] Several metal borohydrides are known to provide high H_2-capacity, however, issues such as: (1) high thermodynamic stability [e.g. high desorption temperature for $LiBH_4$ or $Mg(BH_4)_2$],[7,8] (2) thermodynamic instability [as seen in $Ti(BH_4)_2$ and $Cu(BH_4)_2$],[9,10] and (3) release of highly dangerous or toxic by-products, such as BeH_2, B_2H_6 [$Be(BH_4)_2$, $Al(BH_4)_3$ and $Zn(BH_4)_2$],[11-13] have thus far limited their success as suitable hydrogen storage candidates. It has been shown that there are ways in which to overcome these challenges, such as utilizing doping[14] or the identification of catalysis,[15] etc. Nevertheless, the utilization of additive agents imposes a penalty on hydrogen capacity to a level that is unacceptable for practical application. Thermodynamic modification of metal hydrides is considered to be an appropriate approach to reduce the operating temperature due to the driving force of $H^{\delta+}/H^{\delta-}$ combination.[16] In recent years, such an approach has been widely adopted by different research groups to destabilize the Li(Mg, Ca)–B-N–H system; this has resulted in a significant decrease in the reaction enthalpy and a low dehydrogenation onset temperature compared to the individual constituent.[17,18]

Ammonia borane (AB) and its related compounds, are another series of materials generating intense interest as hydrogen sources.[19] It is widely accepted that an attractive interaction between $H^{\delta+}$ and $H^{\delta-}$ is responsible for the hydrogen molecule being desorbed at low temperature.[19] More recently, ammine metal borohydrides (AMBs), another B-N-based hydride system, have been investigated with respect to their thermal decomposition properties, their crystalline structure and mechanism of H-evolution.[20-24] In AMBs, the ammonia is coordinated with the metal cation of borohydrides, which is similar to the ammine metal salts.[25] The distinguished performance of AMBs regarding hydrogen storage can be ascribed to the combination of the NH_3 group and the BH^{4-} anion on a molecular level. NH_3 and BH^{4-} groups have a number of favorable attributes including, a high hydrogen capacity, 17.6 wt. % for NH_3 and 26.7 wt.% for BH^{4-}; and highly mobile Hδ+/Hδ- atoms which may lead to a rapid generation of H_2 and subsequent desorption at low temperature.[26, 27] However, despite their promising characteristics, it has been observed that across a range of AMBs they display a variety of different thermal decomposition properties. $LiBH_4 \cdot NH_3$ and $Ca(BH_4)_2 \cdot 2NH_3$ mainly release ammonia rather than hydrogen during decomposition in argon, which is attributed to the weak coordination between Li^+ (Ca^{2+}) with NH_3 in the material.[21, 22] In order to promote their dehydrogenation performance, chemical modification with various metal hydrides or metal chlorides or thermal decomposition under ammonia atmosphere are required.[22,23] On the contrary, $Mg(BH_4)_2 \cdot 2NH_3$ and $Al(BH_4)_3 \cdot 6NH_3$ and its double cation complex show dominant hydrogen release upon heating. This is particularly true of the aluminum-based complexes [20, 24] which are able to release over 10% hydrogen below 150 °C, exhibiting their potential as an advanced solid state hydrogen storage substrate. The above results strongly suggest that the dehydrogenation of AMBs is dependent on the central metal cation(s), which affect the bonding properties between BH_4 and NH_3 and thus lead to different dehydrogenation behavior. Therefore, development of AMBs requires a better understanding of the crystal and electronic structures of the materials in order attempt targeted design and to further improve characteristics such as the dehydrogenation temperature, purity of gas released, and

thermodynamic properties.

Along with Mg^{2+} and Al^{3+}, Zn^{2+} is also able to form strong coordination bonds with ammonia, which suggests potential for favorable dehydrogenation of ammonia complexes of the Zinc borohydride system.[28-31] As early as 1959, zinc tetrahydroborate amines ($Zn(BH_4)_2{\cdot}4NH_3$) could be obtained from aqueous-ammoniacal solutions at low temperature by exchange reaction between the metal salts and sodium tetrahydroborate.[31] However, to the best of our knowledge, there have been no reports on the formation of $Zn(BH_4)_2{\cdot}2NH_3$ and dehydrogenation properties of this class materials. In this paper, we report the synthesis and detailed structural, physical, and chemical characterization of the new ammine borohydride-based material $Zn(BH_4)_2{\cdot}2NH_3$. Our results show that the dehydrogenation properties of $Zn(BH_4)_2{\cdot}2NH_3$ are significantly improved in terms of dehydrogenation temperature, hydrogen capacity, and the purity of gas released compared to the other reported ammine metal borohydrides. In addition, density functional theory results relating to this compound are compared to results from similar calculations for $Ca(BH_4)_2{\cdot}2NH_3$ and $Mg(BH_4)_2{\cdot}2NH_3$ and hydrogen release properties of these materials are discussed.

Experimental

Sample and equipments

$LiBH_4$ (95%, J&K Co. Ltd), liquid anhydrous ammonia (99.999%, Sinopharm Chemical Reagent Co. Ltd) and anhydrous $ZnCl_2$ (99.99%, Sigma Aldrich Co. Ltd) were all sourced commercially. In order to produce pure $ZnCl_2{\cdot}2NH_3$, $ZnCl_2{\cdot}6NH_3$ was pre-fabricated by exposing $ZnCl_2$ powder in 1 atm ammonia for 24 hours and then thermally decomposing the product to $ZnCl_2{\cdot}2NH_3$ and NH_3 under Ar flow at 150 °C. The composition of $ZnCl_2{\cdot}2NH_3$ was identified by gravimetry. XRD results (Figure S1) revealed that the synthesized $ZnCl_2{\cdot}2NH_3$ structure is orthorhombic (space group Imam) with lattice parameters a = 7.7025(2) Å, b = 8.1005(3) Å and c = 8.5051(3) Å, which is consistent with that reported in literature.[32] $Zn(BH_4)_2{\cdot}2NH_3$ was prepared by milling the mixture of $LiBH_4$ and $ZnCl_2{\cdot}2NH_3$ in a 2:1 molar ratio for 60 min (planetary QM-1SP2) at 400 rpm under argon using stainless steel spheres with a BPR of 60:1. The milling process was carried out alternating 6 min of milling and 6 min of rest in order to avoid an unacceptable increase in the temperature of the powders in the vial. By way of comparison, $ZnCl_2/2LiBH_4$ was also processed under the same conditions as described above. All handling of the powders before and after milling were carried out in a glove box containing an argon atmosphere. Gas release property measurements were performed by thermogravimetry analysis connected to a mass spectrometer (TGA-MS), using a heating rate of 10 °C min^{-1} under 1 atm Nitrogen with a purge rate of 200 cm^3 min^{-1}. To identify all possible gaseous products, survey scans in the mass range of 2-80 amu were recorded from the two samples. The temperature dependence of desorption/decomposition was monitored by a Sievert's temperature-programmed-desorption (TPD) under 1 atm argon.

High-resolution X-ray powder diffraction data were collected from $Zn(BH_4)_2{\cdot}2NH_3$ samples at the Australian Synchrotron powder diffraction beamline,[33] using the Mythen-II detector.[34] For phase identification and structure determination, the sample was loaded into a pre-dried 0.5 mm special-glass capillary whilst inside an Argon-filled glove box. The capillary was sealed with vacuum grease for X-ray diffraction measurements. High temperature in-situ XRD were conducted using a Cyberstar hot air blower at a heating rate of 3 °C min^{-1}; and data were collected over the temperature range 25 to 430 °C, in steps of 5 °C. For in-situ high temperature measurements, the sample was loaded into a 0.7 mm quartz capillary and mounted in a gas flow-cell in order to maintain an argon atmosphere over the sample throughout the experiment. Data were collected for all measurements at a wavelength of 0.8260 Å, determined through the use of NIST standard LaB6 660a. Solid-state infrared spectra of the samples (as KBr pellets) were recorded on a Nicolet Nexus 470 in the range of 300 cm^{-1} to 4000 cm^{-1}. During the IR measurement, samples were loaded into a sealed tube with CaF_2 windows. Solid-state ^{11}B NMR data were recorded (DSX 300) using a Doty CP-MAS probe with no probe background. All of those solid samples were spun at 12 kHz, using 4 mm ZrO_2 rotors filled under a purified argon atmosphere within a glove box. A 0.55 μs single-pulse excitation was employed, with repetition times of 1.5 s. Differential scanning calorimetry (DSC) was performed by netzsch 204HP DSC under argon with a gas flow of 20 ml min^{-1} at a heating rate of 10 K min^{-1}. The N and H elemental analyses were performed using an Elementar Vario EL-III instrument. The isothermal dehydrogenation performances of the samples were examined by TPD apparatus with typical sample weigh of 90 mg. For comparison, the TG and TPD results relative to the pure $Zn(BH_4)_2{\cdot}2NH_3$ are also showed in this study.

Sample and equipments

The geometries of $Me(BH_4)_2{\cdot}2NH_3$ (Me = Zn, Ca or Mg) have been optimized by first principles calculations with the CASTEP code[35, 36] based on density functional theory (DFT). The Perdew Burke Ernzerhof (PBE) functional was used with the generalized gradient approximation (GGA) for all calculations.[37] The ultrasoft pseudopotentials that we used have the valence-electron configurations of $1s^1$ (core radius 0.8 a. u.) for H, $2s^22p^1$ (core radius 1.4 a. u.) for B, $2s^22p^3$ (core radius 1.4 a. u.) for N, $3d^{10}4s^2$ (core radius 2.0 a. u.) for Zn, $2p^63s^2$ (core radius 2.06 a. u.) for Mg and $3S^22p^64S^2$ (core radius 1.6 a. u.) for Ca. The initial $Me(BH_4)_2{\cdot}2NH_3$ structures for optimization were taken from the X-ray refinement data directly. We have used the plane-wave cut-off of 500 eV for representing the wave functions and 4 x 3 x 4 k-

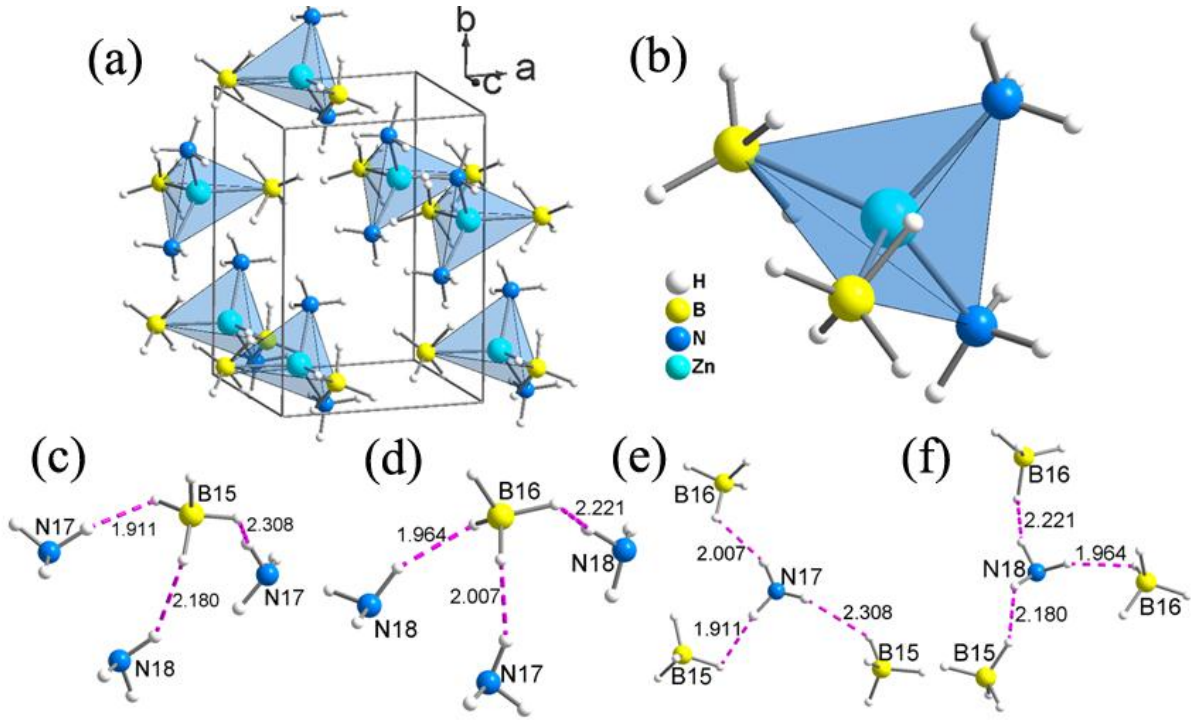

Fig. 1 Illustrations of the $Zn(BH_4)_2{\cdot}2NH_3$ structure: (a) 'molecular' fragment; and (b) 2×2×2 unit cell projected down the *c*-axis.

point grid (i.e. 24 k-points) for the Brillouin zone sampling by the Monkhorst–Pack scheme. Geometry optimizations were performed using the BFGS procedure 38 at 0 K. The energy tolerance was 5×10^{-6} eV/atom; the maximum tolerance for force and atom displacements along any Cartesian component was 0.01 eV/Å and 5×10^{-4} Å, respectively. These parameters lead to a satisfactory convergence of the total energy. Geometry optimization was conducted in this study with the full optimization. The calculated structure files (ZnBNH-2-opt.cif) are attached in the supplementary information. The fully-optimized structure was selected for further exploration and was used to calculate density of states (DOS) and the electron localization function (ELF) information.

Results and discussions

Synthesis and Crystal structure determination

Our proposal to synthesize $Zn(BH_4)_2(NH_3)_2$ stems from the early report regarding $Zn(BH_4)_2$ preparation by solution chemistry:[12(b), 39]

$$2MBH_4+ZnCl_2 \xrightarrow{Et_2O} Zn(BH_4)_2+2MCl \quad (1)$$ (M=K, Li or Na)

Given Zn^{2+} in $Zn(BH_4)_2$ is a soft Lewis acid as compared to alternatives such as Li^+, and Na^+ which are hard acids,[12(b)] the desired metathesis reaction should occur by substituting the starting material of $ZnCl_2$ in Eqn. (1) with $ZnCl_2{\cdot}2NH_3$, as described in Eqn. (2).

$$ZnCl_2{\cdot}2NH_3+2LiBH_4 \xrightarrow{\text{ball milling}} Zn(BH_4)_2{\cdot}2NH_3+2LiCl \quad (2)$$

The product of this reaction has been verified by XRD, FTIR and element analysis (N, H). Elemental analysis confirms that there is no appreciable change in the ratio of N to H (before ball milling, N:H=1:7; and after ball milling, N:H=1:6.65), indicating no loss of NH_3 sources during the ball milling. This study reports the structure of $Zn(BH_4)_2{\cdot}2NH_3$ which has been solved by synchrotron radiation powder X-ray diffraction. (Structural data and atomic position are summarized in Table S1-S3, respectively). Bragg peaks in the room temperature diffraction patterns from the sample were indexed to a monoclinic unit cell using the program DICVOL.[40] The space group $P2_1$ and $P2_1/m$ can be assigned based on systematic absences. The structure was subsequently solved in the space group of $P2_1$ (No. 4) by global optimization in direct space, using the program FOX.[41] Rietveld refinement was performed using TOPAS v4.2, [42] and the refined lattice parameters are a = 6.392(4) Å, b = 8.417 (6) Å, c = 6.388(4) Å, β = 92.407(4)°. The diffraction profile fit using these parameters is shown in Figure S2; the Rietveld fit line and differences between the experimental and calculated values are visible.

The structure of $Zn(BH_4)_2{\cdot}2NH_3$, as shown in Figure 1, can be described as comprising discrete units of $Zn(BH_4)_2{\cdot}2NH_3$ where zinc cations are coordinated by $2NH_3$ and $2BH_4$, similar to the interactions observed in $Mg(BH_4)_2{\cdot}2NH_3$ where the structure is described as essentially molecular.[20] The observed average Zn-N distance, of 2.13 Å, is a little longer than that in $ZnCl_2{\cdot}2NH_3$ at 2.02 Å.[32] The difference in the structures of these two complexes is evidently not caused by steric factors (the ionic radius of the BH_4^- group is close to that of Cl^-) but rather the possible formation of Cl-N hydrogen bonds in the latter.[43] The Zn-B average distance of 2.32 Å is quite close to the corresponding contact in $Mg(BH_4)_2{\cdot}2NH_3$ (2.39 Å) for the pseudotetrahedral coordinated Mg atom.[20] In addition, the packing of $Zn(BH_4)_2{\cdot}2NH_3$ is highly consistent with that observed in $Mg(BH_4)_2{\cdot}2NH_3$, the N_2 edge of one molecule faces one B atom of another molecule. These interactions lead to the arrangement of the $Zn(BH_4)_2{\cdot}2NH_3$ molecules into pseudo-layers perpendicular to the a axis. The Zn-H bonds in $Zn(BH_4)_2{\cdot}2NH_3$, at 1.9 Å, are shorter by *ca*. 0.2 Å, than those reported for the

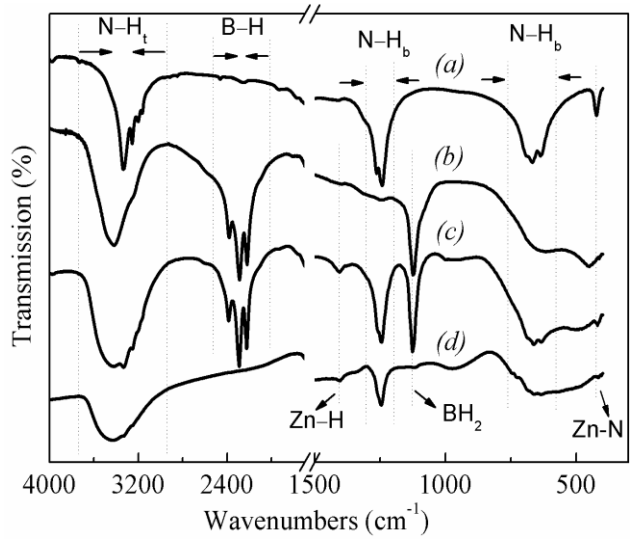

Fig. 2 FTIR spectra from reagents (a) $ZnCl_2{\cdot}2NH_3$ and (b) pure $LiBH_4$. FTIR spectra from the product (c) post-milled $ZnCl_2{\cdot}2NH_3/2LiBH_4$ and (d) post-heated $ZnCl_2{\cdot}2NH_3/2LiBH_4$. Regions of the spectra have been marked to denote relevant features pertaining to the structures.

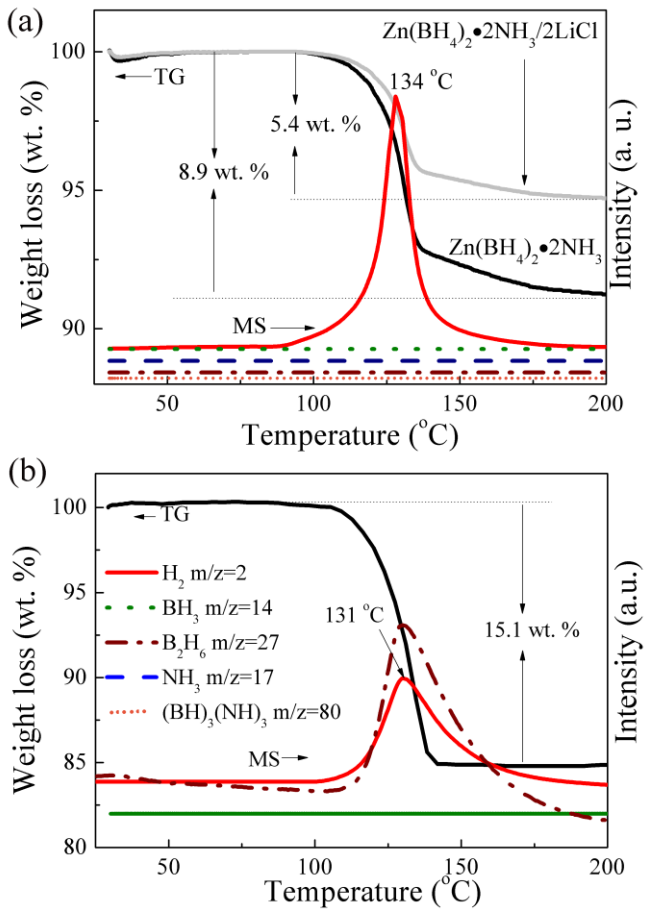

Fig. 3 TG-MS profiles for the as-prepared $Zn(BH_4)_2{\cdot}2NH_3$ (a) and $2LiBH_4/ZnCl_2$ (b). For comparison, the TG results relative to the $Zn(BH_4)_2{\cdot}2NH_3/2LiCl$ and pure $Zn(BH_4)_2{\cdot}2NH_3$ are showed in (a), respectively).

$Zn_2(BH_4)_5^-$ ion.[39] This observation is supported by FTIR data as shown in Figure S3, which also shows a formed weakening of the Zn-H bond relative the reported Zn-H bond in $Zn(BH_4)_2$. Such weakening may be caused by the steric effects of NH_3 group in $Zn(BH_4)_2{\cdot}2NH_3$. Furthermore, the much shorter H-H distances (1.91-2.31 Å, Table S4) from $Zn(BH_4)_2{\cdot}2NH_3$ suggest the formation of dihydrogen bonding as addressed in other AMBs compounds.[20-23] As shown in Figure 1c, d, e, and f, $Zn(BH_4)_2{\cdot}2NH_3$ comprises $H^{\delta+}$ from NH_3 units and $H^{\delta-}$ from BH_4 units indicating the high possibility to possess of strongly hybridized valence electrons or closed shell bonds between B-H and between N-H, which can be primarily responsible for stability of this structure at room temperature. The strong NH···HB interaction in $Zn(BH_4)_2{\cdot}2NH_3$ structure is also expected to have a great impact on improving the dehydrogenation performance.

It is reported that the preparation of neat $Zn(BH)_4$ using dry chemistry such as ball milling can be hindered by the tendency toward formation of mixed-cation (Zn-Li or Zn-Na) borohydrides.[44] By analogy, it is also possible for the formation of $LiZn(BH_4)_3{\cdot}2NH_3$ in the reaction of Eqn.(2). We tried to solve the structure on both $LiZn(BH_4)_3{\cdot}2NH_3$ and $Zn(BH_4)_2{\cdot}2NH_3$ chemical formula with all possible space groups with the relatively small volume (343.4Å^3). However, with $LiZn(BH_4)_3{\cdot}2NH_3$ composition, the additional Li atom and BH_4 group can not fit into the indexed monoclinic unit cell with overestimated density. In addition, if the final product is the formation of $LiZn(BH_4)_3{\cdot}2NH_3$, $ZnCl_2{\cdot}2NH_3$ would be excessive. However, form the XRD results, no $ZnCl_2.2NH_3$ can be identified after ball milling (Figure S2). These results indirectly confirm that the formed ammoniate is the $Zn(BH_4)_2.2NH_3$ rather than $LiZn(BH_4)_3.2NH_3$.

To improve the knowledge about the chemical bond information of $Zn(BH_4)_2{\cdot}2NH_3$, we have carefully examined this new phase by FTIR spectroscopy, before and after heat treatment, and have also obtained FTIR data from the reagents, $ZnCl_2{\cdot}2NH_3$ and $LiBH_4$, for comparison (Figure 2). Features in the spectra pertaining to the starting materials are evident in the spectrum recorded from the post-milled sample, suggesting that both B and N atoms are still in the integral ligation pattern BH_4^- and NH_3 group.[39] Thus, although it is normally believed that it is not possible to locate H-atom positions from powder XRD data, this FTIR information, which is highly consistent with original NH_3 and BH_4, lend credence to the rigid body modeling of BH_4^- and NH_3 groups. Moreover, Zn-N bonding can be clearly observed in Figure 2c, following milling, at the same wavenumber as in $ZnCl_2{\cdot}2NH_3$, implying that the Lewis acid to which NH_3 coordinates is still Zn^{2+}. The bond length, as determined by powder diffraction is longer in $Zn(BH_4)_2{\cdot}2NH_3$ (at *ca*. 2.13 Å) compared to that in $ZnCl_2{\cdot}2NH_3$ (at 2.02 Å),[32] agreeing well with the decreasing intensity of IR absorption following milling. Notably, after ball milling of $ZnCl_2{\cdot}2NH_3$ and $LiBH_4$, the appearance of a weak peak observed in 1409 cm^{-1} (nearly exactly the position of the reported Zn-H vibration, see Figure S3)[39] suggests that, by mechanochemical reaction, BH_4^- transfers from $LiBH_4$ to combine with Zn^{2+} and engages in a substitution reaction with Cl^-. The above results directly confirm some key information about $Zn(BH_4)_2{\cdot}2NH_3$, namely, that both the BH_4^-

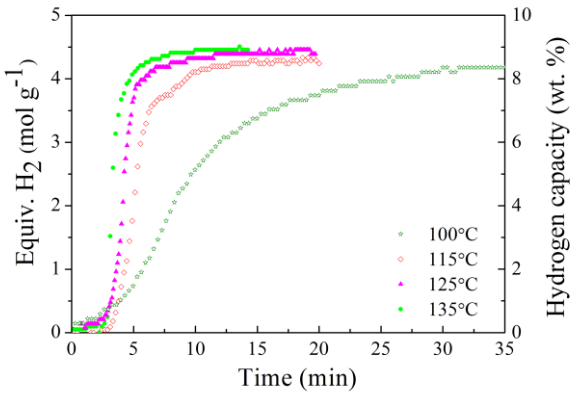

Fig. 4 Isothermal curves for hydrogen desorption of $Zn(BH_4)_2{\cdot}2NH_3$ at various temperatures. The results are calculated relative to the pure $Zn(BH_4)_2{\cdot}2NH_3$.

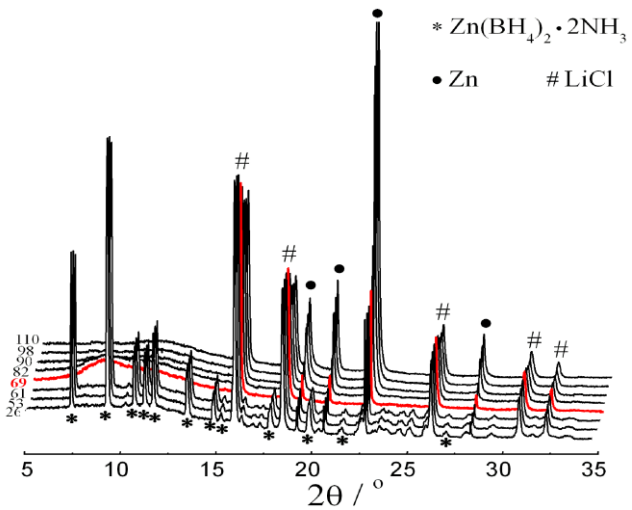

Fig. 5 In-situ variable temperature high resolution powder XRD data collected from $Zn(BH_4)_2{\cdot}2NH_3$. The compound was heated to selected temperatures at fine temperature steps. Asterisks (*) mark the position of $Zn(BH_4)_2{\cdot}2NH_3$ diffraction peaks, peaks relating to impurities are also indicated.

and the ligand NH_3 subunits remain intact in the new structure; and Zn^{2+} is observed to have bonded with both the NH_3 and BH_4^- groups.

Dehydrogenation performance and pathway

In order to emphasize the positive effect of the coordinated NH_3, $ZnCl_2/2LiBH_4$ was milled together under the same condition as $ZnCl_2{\cdot}2NH_3/2LiBH_4$ and laboratory XRD data were acquired to confirm the identity of the synthesized phase (see Figure S4). According to the previous literatures, the ball milled products of $ZnCl_2/2LiBH_4$ turn out to be a mixed-metal (Zn-Li) borohydride ($ZnLi(BH_4)_3$).[44] Figure 3 shows the thermal decomposition performance of the as-prepared $Zn(BH_4)_2{\cdot}2NH_3$ compared to the as-prepared $ZnLi(BH_4)_3$. As seen from the mass spectrometry (MS) profiles(Figure 3a), the H_2 desorption from $Zn(BH_4)_2{\cdot}2NH_3$ starts at around 90 °C and ends before 150 °C with one peak centered at 127 °C, and no ammonia, boranes and borazine impurities were detected throughout the heating. By contrast, the MS results of the ball milled $ZnCl_2/2LiBH_4$ confirm that a significant volume of diborane, B_2H_6, accompanies the evolution of H_2, leading to a large mass loss of 15.1 wt.% (Figure 3b). Furthermore, the quantity of H_2 released (about 5.7 equiv., see Figure S5) before 200 °C determined by volumetric measurement agrees very well with the value calculated based upon to the TGA result (ca. 5.74 mole H_2), which shows a weight loss of 8.9 wt.% for pure $Zn(BH_4)_2{\cdot}2NH_3$ (accounting for 5.36 wt.% in $Zn(BH_4)_2{\cdot}2NH_3/2LiCl$ mixture). Clearly, the adduct of NH_3 plays a crucial role in ensuring the purity of H_2 and suppressing B_2H_6 release. Furthermore, the dehydrogenation of $Zn(BH_4)_2{\cdot}2NH_3$ was investigated using isothermal volumetric hydrogen release measurements at various temperatures. As shown in Figure 4, approximately 5.5 equiv. hydrogen can be released within 35 min at 100 °C, suggesting favorable kinetics for this hydrogen storage material. Using increasing temperatures, from 115 °C to 135 °C, hydrogen release time can be reduced from 15 min to 10 min, respectively. This faster release is accompanied by an increase in the volume of hydrogen released, to *ca.* 5.7 equiv. hydrogen, corresponding to 8.9 wt.% at 115 °C.

The differential scanning calorimetry (DSC) results from the thermal decomposition of $Zn(BH_4)_2{\cdot}2NH_3$ (Figure S6) reveal that the decomposition is preceded by one small endothermic signal which occurs without any mass loss between 72-90 °C, originating from the melting of $Zn(BH_4)_2{\cdot}2NH_3$. This melt point was visually confirmed by heating $Zn(BH_4)_2{\cdot}2NH_3$ in an Argon filled transparent vial. A maximum exothermic peak appeared at ca. 131 °C, corresponding to the release of hydrogen. Integration of the differential heat in the range of 90-160 °C yields a heat of decomposition of approximately -15 kJ mol^{-1} H_2, which is lower than that of AB (-21 kJ mol^{-1} H_2).[45] Although the exothermic dehydrogenation of $Zn(BH_4)_2{\cdot}2NH_3$ suggests that a direct reversibility of rehydrogenation from the decomposed products is infeasible, recent results on the reversible rehydrogenation via a chemical route conducted in AB system[46] illuminate the possibility of a more feasible chemical reversibility of $Zn(BH_4)_2{\cdot}2NH_3$ due to its lower exothermicity than AB upon decomposition.

From the *in-situ* X-ray diffraction data shown in Figure 5, the changes undergone by the sample are reflected in the diffraction data and can be correlated to melting and H_2 desorption observed in the MS and DSC results. At 26 °C, the as-prepared $Zn(BH_4)_2{\cdot}2NH_3$ can be clearly identified with intense and sharp Bragg diffraction peaks in the angle range of 5-30 degrees, indicative of long-range crystalline order of the material. Aside from the presence of LiCl, which is a by-product of $Zn(BH_4)_2{\cdot}2NH_3$ synthesis, a number of peaks with relatively weak intensity relating to Zn are also observed; these suggest the fractional decomposition of $Zn(BH_4)_2{\cdot}2NH_3$ due to the ball milling. Fractional decomposition is supported by ^{11}B NMR results which show small B-N-H peaks (see Figure S7). As the temperature increases during the diffraction experiment the data reveal an abrupt absence of $Zn(BH_4)_2{\cdot}2NH_3$ and the presence of

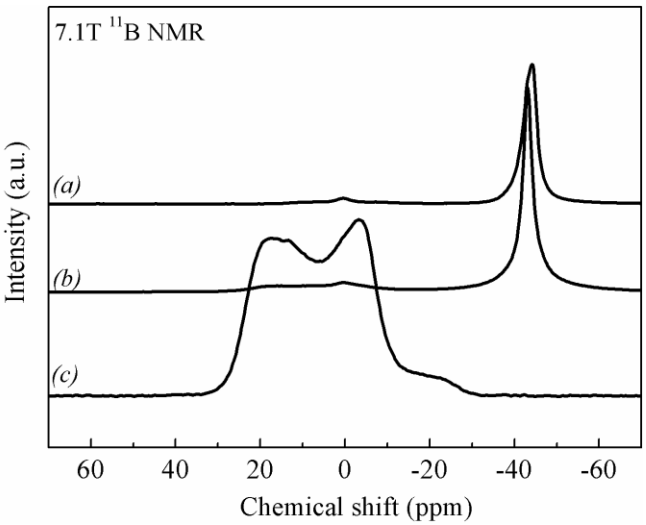

Fig. 6 ^{11}B NMR of (a) post-milled $Zn(BH_4)_2{\cdot}2NH_3$ and following heating to (b) 100 °C and (c) to 200 °C. The heat rate was 10 ^{o}C min^{-1}.

an amorphous phase, at *ca.* 69 ^{o}C due to the melting of $Zn(BH_4)_2{\cdot}2NH_3$. We note that the similar phase change (solid to viscous liquid) is also observed in the dehydrogenation process of $Mg(BH_4)_2{\cdot}2NH_3$.[20] It suggests that with the temperature increase some similar amorphous intermediate(s), e.g. the B-N cleavage, may occur before H_2 release in both $Zn(BH_4)_2{\cdot}2NH_3$ and $Mg(BH_4)_2{\cdot}2NH_3$. As the temperature increases further the psuedomolecular structure of $Zn(BH_4)_2{\cdot}2NH_3$ continues to decompose and the intensity of the Zn peaks increase until they reach a maximum at around 110 ^{o}C. Decomposition of $Zn(BH_4)_2{\cdot}2NH_3$ with hydrogen release starts at *ca*. 90 ^{o}C; no crystalline phases are observed, however, an amorphous form of $Zn(BH_4)_2{\cdot}2NH_3$ may be an intermediate phase and Zn is therefore the only crystalline product in this H_2-desorption process. It is worth noting that the role of LiCl in the dehydrogenation of $Zn(BH_4)_2{\cdot}2NH_3$ has yet to be demonstrated or ruled out; however, this investigation relies on developments in phase separation and sample purification. It is believed that the imperceptible changes in peak intensity and width pertaining to LiCl in the in-situ XRD patterns may imply that there is no interaction between $Zn(BH_4)_2{\cdot}2NH_3$ and LiCl.

The fact that only Zn can be observed for the decomposed $Zn(BH_4)_2{\cdot}2NH_3$ (Figure 5) indicates that any other decomposition products which may have formed could only be present as amorphous phases. FTIR results reveal that, all of the B-H bonds, including B-H bending and stretching modes, are almost undetectable for the decomposed $Zn(BH_4)_2{\cdot}2NH_3$ (Figure 2), while the other signals, including Zn-H, N-H and Zn-N, occur at the same position but decrease in intensity. The surviving absorption peaks imply that the final amorphous compound should consist of Zn-H, N-H and Zn-N bonds. The solid-state ^{11}B NMR results provided some additional valuable hints in the composition evolution and hydrogen release process of $Zn(BH_4)_2{\cdot}2NH_3$. Figure 6 shows ^{11}B NMR results for the as-prepared sample which reveal a primary boron species with a chemical shift of -44.1 ppm; this is assigned to the boron nucleus in the tetrahedral BH_4^- units.[47] Meanwhile, one comparatively weak peak is observed at 0.4 ppm, indicating that detectable changes occurred in the chemical environment of the B atoms compared to the BH_4^- molecules derived through mechanical milling. This, again, suggests the possibility of partial decomposition of $Zn(BH_4)_2{\cdot}2NH_3$ (see Figure S7). After heat treatment to 100 °C, one weak peak at 15.0 ppm was observed along with the peak of 0.4 ppm (see Figure S7). The appearance of these two weak peaks suggests that the chemical environment of fractional B atom shifts to the lower fields intensively compared to the tetrahedral BH_4^- since the formation of HBN_2 and/or BN_3.[48] In addition, the chemical shift, which is assigned to

Table 1. Summarization of calculated crystal structures and selected atomic distances of $Me(BH_4)_2{\cdot}2NH_3$ (Me=Zn, Mg, Ca).

	$Zn(BH_4)_2{\cdot}2NH_3$	$Mg(BH_4)_2{\cdot}2NH_3$	$Ca(BH_4)_2{\cdot}2NH_3$
Crystal system	monoclinic	orthorhombic	orthorhombic
Space-group	P 1 21 1 (4)	P b c a (61)	P b c n (60)
Cell parameters	a=6.4919 Å	a=9.3612 Å	a=6.4728 Å
	b=8.8878 Å	b=17.9632 Å	b=8.2730 Å
	c=6.4625 Å	c=8.7252 Å	c=12.4126 Å
	β=91.8200°		
M-H	1.887	2.026	2.414
	1.897	2.058	2.469
	1.956	2.191	2.515
	2.590	2.655	2.987
	2.623	2.663	3.089
M-B	2.281	2.261	2.769
	2.286	2.394	2.960
M-N	2.078	2.140	2.517
		2.142	
H-H	1.905	2.081	2.026
	2.003	2.192	2.332
	2.177	2.230	2.438

BH_4^-, is still observed at -43.1 ppm. [47] Upon further heating to 200 °C, the peaks corresponding to HBN_2 and/or BN_3 (observed at 17.4 ppm and -3.1 ppm) increased in intensity which coincides with the peak of BH_4^- diminishing totally (Figure 6c). By combination of the XRD, FTIR, NMR and elementary analysis of the end-products (N: H ratio is 1:1) results, as well as the thermolysis results, the dehydrogenation of $Zn(BH_4)_2 \cdot 2NH_3$ can be speculated as:

$$2Zn(BH_4)_2 \cdot 2NH_3 \rightarrow Zn + Zn(BNH)_2 + 13H_2 \quad (2)$$

The calculated weight loss of the Eqn. (2) is ca. 10 wt.%, 1.1 wt.% higher than the experimental result, which can be explained by a fraction of decomposition of $Zn(BH_4)_2 \cdot 2NH_3$ during the ball-milling, demonstrated by the XRD and ^{11}B NMR results (Figure S2 and Figure S7). From the results above, it is concluded that the dehydrogenation mechanism of $Zn(BH_4)_2 \cdot 2NH_3$ could be generally traced to the combination of the positive and negative H atoms from [NH] and [BH] sources, respectively. However, On condition that a balanced reaction of BH and NH occurs in the $Zn(BH_4)_2 \cdot 2NH_3$, the final products should remain excessive BH groups. This is opposite to the IR results, which gives the evidence of residual NH groups but not BH groups. Therefore, a H transfer from B to N may occur in $Zn(BH_4)_2 \cdot 2NH_3$ upon dehydrogenation. Anyhow, the dehydrogenation pathway of ammoniates of Zn-based borohydrides is somewhat different with the other reported AMBs, [20-23] e.g. $Mg(BH_4)_2 \cdot 2NH_3$, in which the metal cations in the dehydrogenated products are always bonded to the BN species.

Electronic structure and chemical bonding analysis

In order to gain a better understanding of the structure and dehydrogenation properties of $Zn(BH_4)_2 \cdot 2NH_3$, we compare it with two other similar compounds, which are summarized in Table 1. By comparing the Me-H and Me-N (Me = Ca, Mg or Zn) interatomic distances of these materials, it is possible to correlate the structural features of these materials with the dehydrogenation performance. The average distance of Ca-H in $Ca(BH_4)_2 \cdot 2NH_3$ is 2.414 Å. While in $Mg(BH_4)_2 \cdot 2NH_3$, that distance is ca. 2.026 Å. In $Zn(BH_4)_2 \cdot 2NH_3$, the average distance is significantly lower, at 1.887 Å. In each case the metal cation is similarly coordinated and the ionic radii of Ca^{2+}, Mg^{2+}, and Zn^{2+} are 100, 72 and 74 pm, respectively. Thus, the hydrogen atoms bonded to boron are expected to show increasing anionic character with decreasing Me-H bond distance, in the order of $Ca(BH_4)_2 \cdot 2NH_3$, $Mg(BH_4)_2 \cdot 2NH_3$ to $Zn(BH_4)_2 \cdot 2NH_3$. Thereby, affording $Zn(BH_4)_2 \cdot 2NH_3$ improved dehydrogenation capacity. The Zn-N and Mg-N average distances are comparable in $Me(BH_4)_2 \cdot 2NH_3$ with distances of 2.078 Å and 2.142 Å, respectively. While the Ca-N distance is surprisingly long, at 2.517 Å, which may contribute to the ammonia detachment under inert atmosphere[21] and therefore poor dehydrogenation performance.

The calculated electronic density of states (DOS) (Figure 7) show all structures have a similar finite energy gap in general (Zn 4.8 eV, Mg 4.9 eV, Ca 5.1 eV), therefore they all exhibit non-metallic features. All calculated DOSs show similar features. From the projected DOS plots, it can be seen that the lower valence band (VB, -16 to -10 eV) is dominated by N electrons and H electrons in all three compounds. The middle VB, (-10 to -5 eV) is dominated by N states, B states and H states in all three compounds, indicating effective overlapping and forming of very strong bonds. This is consistent with the following analysis of the electron localization function plots, *i.e.*, the high ELF value near B-H and N-H atoms. Furthermore, in the upper VB region (-5 to 0 eV), metal (Mg, Ca, Zn), B, N and H electrons dominate, indicating strongly hybridized B-N-H states, which suggests that metal atoms have some interaction with the surrounding atoms. Mg and Ca electrons have negligible contribution near the Fermi energy, while Zn elections have a larger contribution. It should be noted that Zn has high states in the -5 to -3 eV VB range, which overlaps with B-N-H states, indicating that Zn forms bonds with surrounding atoms. This may explain the favorable dehydrogenating properties of $Zn(BH_4)_2 \cdot 2NH_3$ comparing with $Ca(BH_4)_2 \cdot {}_2NH_3$ and $Mg(BH_4)_2 \cdot 2NH_3$. In the conduction band (CB), the main contributions are from metal, B and H atoms, while N contributes negligibly to the CB.

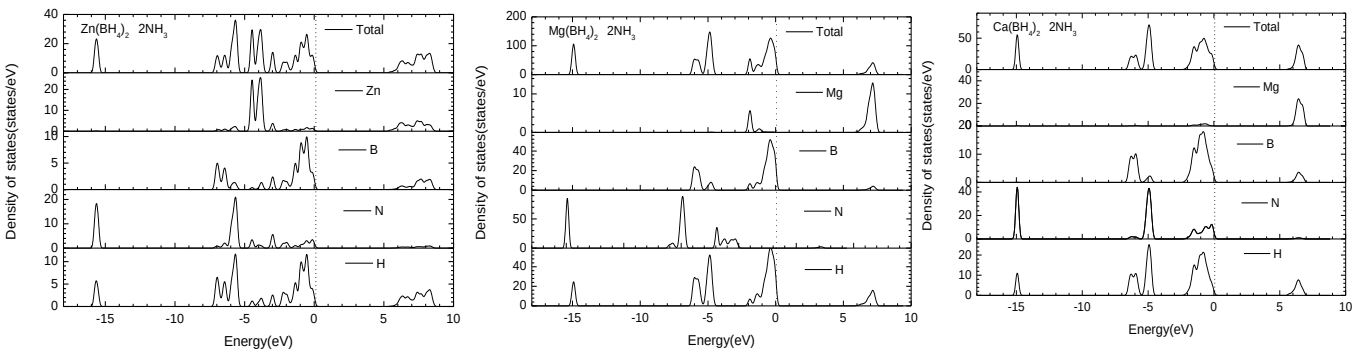

Fig. 7 Electronic density of states for $Zn(BH_4)_2 \cdot 2NH_3$, $Mg(BH_4)_2 \cdot 2NH_3$ and $Ca(BH_4)_2 \cdot 2NH_3$. Total DOS results are shown for each material, followed by DOS results for M, B, N, and H.

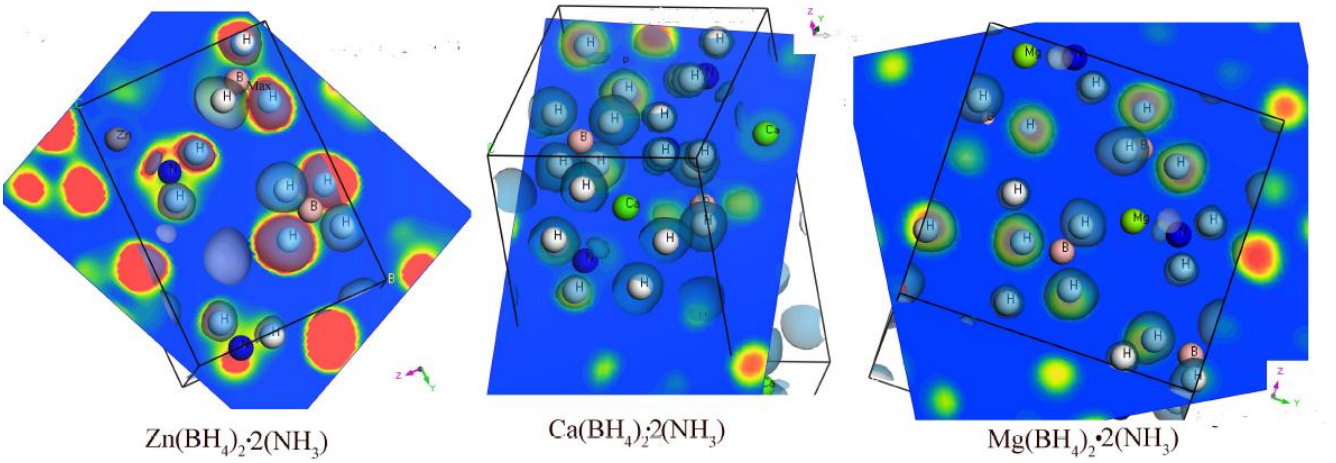

Fig. 8 Electron localization function (ELF η) for $Zn(BH_4)_2{\cdot}2NH_3$, $Mg(BH_4)_2{\cdot}2NH_3$ and $Ca(BH_4)_2{\cdot}2NH_3$. An isosurface of η = 0.15 has been used in all figures, 2D cross section cut through M, B, N, and H atoms.

Table 2. Summary of dehydrogenation peak temperature (D_p), Pauling electronegativity (χ_p) and H_2 and NH_3 evolution for $Zn(BH_4)_2{\cdot}2NH_3$, $Mg(BH_4)_2{\cdot}2NH_3$, and $Ca(BH_4)_2{\cdot}2NH_3$.

Samples		$Zn(BH_4)_2{\cdot}2NH_3$	$Mg(BH_4)_2{\cdot}2NH_3$	$Ca(BH_4)_2{\cdot}2NH_3$
χ_p		1.65	1.31	1.0
Dp (/°C)		127	~200	~280[a]
H_2 released (wt. %)	Observed	8.9[b]	12.3~13.1	12.3[a]
	Calculated	10.8[b]	16	13.5
NH_3 released	Observed	0	0~0.8	32.7
	Calculated	26.4	38.6	32.7
References		This paper	[20]	[21]

[a] Nearly no hydrogen releases from $Ca(BH_4)_2.2NH_3$ under the dynamic flow mode, and the listed value is obtained as the dehydrogenation of $Ca(BH_4)_2{\cdot}2NH_3$ conducted in closed vessel under ammonia atmosphere.

[b] The H_2-evolution was estimated based on a pure $Zn(BH_4)_2{\cdot}2NH_3$ sample

In order to further analyse the chemical bonding of the materials, the electron localization function (ELF) has also been calculated as shown in Figure 8. ELF is based on the Hartree-Fock pair probability of parallel spin electrons and can be calculated in density functional theory from the excess kinetic energy density due to Pauli-repulsion.[49, 50] This function produces easily understandable, pictorially informative patterns of chemical bonding and is widely used to describe and visualize chemical bonding in molecules and solids.[50] As described earlier, in the case of Zn or Mg they each directly coordinates with 2 BH_4 groups and 2 NH_3 groups, while each Ca atom directly coordinates with 4 BH_4 groups and 2 NH_3 groups nearby. In Figure 8, the distribution of ELF in all structures shows the high ELF value near B-H and N-H atoms. This indicates strongly hybridized valence electrons or closed shell bonds between B and H and between N and H, i.e. covalent bonding. The spherical shell attractors around the H atoms are highly distorted, indicating H atoms are seen by the surrounding H atoms and have strongly localized electrons. The valence shell of the Mg and Ca atoms in the crystal structures is nearly spherical and with low ELF value, which indicates delocalized electrons, while the Zn shell is slightly distorted indicating interaction with nearby atoms. No additional attractors were found in between B and N atoms. This suggests there is no direct ionic bonding between B and N sites; BH_4 and NH_3 groups are only interacting through bonded H atoms. A feature of note is that an attractor can be seen in between metal and N atoms in all structures, which bias toward the N atom. This can be interpreted as ionic bonding characterization between NH_3 groups and metal atoms.

The decomposition behaviours of these three materials are summarized in Table 2. It can be seen that almost no hydrogen is released from $Ca(BH_4)_2{\cdot}2NH_3$ under the dynamic flow mode, and the listed value is obtained as the dehydrogenation of $Ca(BH_4)_2{\cdot}2NH_3$ conducted in closed vessel under ammonia atmosphere. Favorable dehydrogenation performance is observed in the $Mg(BH_4)_2{\cdot}2NH_3$, which can release total of 13.1 wt % H_2 before 400 °C. Like $Mg(BH_4)_2{\cdot}2NH_3$, the calcium analogue has an equivalent number of BH_4 and NH_3 groups. However, the decomposition of calcium borohydride diammoniate under a flow of inert gas only yields NH_3 and later $Ca(BH_4)_2$; no hydrogen is detected by mass spectroscopy.[21] When conducting volumetric release measurement in a closed vessel, the Ca analogue releases

H_2 instead of NH_3, after sample melting. It is proposed that in a closed vessel NH_3 remains in the vicinity of the $Ca(BH_4)_2$, and thus increases the chance of interaction with BH_4 group.[21] In the case of $Zn(BH_4)_2{\cdot}2NH_3$, 8.9 wt.% hydrogen is released under isothermal conditions at 115 °C within 10 min without any undesirable NH_3 and/or B_2H_6 evolved during the decomposition. As summarized in Table 2, it shows that the dehydrogenation temperature of these AMBs is correlated to the Pauling electronegativity (χ_p) of metal cations, i.e. increased χ_p leads to lower decomposition temperature, suggesting that the χ_p of metal cations may play a crucial role in tuning the dehydrogenation temperature of AMBs. This may be due to more electronegativity of Zn atoms than that of Ca and Mg, which contributes to the increased anionic character of H in B-H and cationic character of H in B-H, and thus leading to easier NH···HB interaction. Therefore, the fact that the $Zn(BH_4)_2.2NH_3$ exhibited even lower dehydrogenation temperature than $Ca(BH_4)_2{\cdot}2NH_3$ and $Mg(BH_4)_2{\cdot}2NH_3$ may attribute to its unique structure characteristic obtained by chemical alteration that incorporates NH_3 with BH^{4-} on a molecular level, which can be detailed as the deliberately introduced dihydrogen bonds and tuned cations electronegativity to adjust the temperature and purity of dehydrogenation. The regularity discussed above may provide further insights into the development of new AMBs with more favourable dehydrogenation performance.

Conclusions

In summary, $Zn(BH_4)_2{\cdot}2NH_3$ has been mechanically synthesized via a simple ball-milling method. The crystal structure of $Zn(BH_4)_2{\cdot}2NH_3$ was solved by high resolution powder X-ray diffraction which has been supported by evidence from infra-red spectroscopy and B^{11} NMR. It has been shown, through DSC and MS, that this novel compound is able to release 8.9 wt.% hydrogen at 115 °C within 10 min without any undesirable gas accompanying this release during decomposition, thereby demonstrating the potential of $Zn(BH_4)_2{\cdot}2NH_3$ for on-board hydrogen storage. Promotion of H_2 evolution in $Zn(BH_4)_2{\cdot}2NH_3$ compared to non-ammonia Zn-base borohydride can be ascribed to the bonded ligand ammonia which is crucial for the prevention of release of B_2H_6. Furthermore, by comparing the crystal structures of $Me(BH_4)_2{\cdot}2NH_3$ (M = Zn, Ca, Mg), it has been shown that Zn-H bonding is remarkably shorter in the Zn analogue, thus leading to increased ionic character of H. A correlation between the decreasing of M-H distance and the enhanced dehydrogenation performance has been observed. The DFT calculations show that Mg and Ca electrons have negligible contribution near the Fermi energy, while Zn elections have considerable contribution; indicating that Zn forms bonding with surrounding N and H(B) atoms, which leads to the increasing reactivity of $H^{\delta-}$ in $Zn(BH_4)_2{\cdot}2NH_3$.The observations of this research demonstrate that the adduct of NH_3, which is close to BH_4^- in molecular level, is an effective chemical approach for lowering the dehydrogenation temperature and restraining the emission of borane from metal borohydrides. Our findings provide useful insights and guidelines for the design and synthesis of novel AMBs for hydrogen storage.

Acknowledgements

This work was partially supported by the National Natural Science Foundation of China (Grant No. 51071047), the PhD Programs Foundation of Ministry of Education of China (20090071110053), the Program for New Century Excellent Talents in Universities (NCET-08-0135) Part of this research was undertaken on the Powder Diffraction beamline at the Australian Synchrotron, Victoria, Australia. FWZ would like to thank the NCI and iVEC for computational resources.

Notes and references

[a] *Department of Materials Science, Fudan University, Shanghai 200433, China. Fax: +86-21-65643685; Tel: +86-21-55664581; E-mail: yuxuebin@fudan.edu.cn*

[b] *Australian Synchrotron, 800 Blackburn Rd, Clayton 3168, Australia*

[c] *Nanochemistry Research Institute, Perth 6845, Curtin University*

† Electronic Supplementary Information (ESI) available: [Crystallographic details, XRD, MS, NMR, DSC, FTIR, and TPD results, including Figures S1-S7 and Tables S1-S4.]. See DOI: 10.1039/b000000x/

1 L. Schlapbach, A. Zuttel, *Nature* 2001, **414**, 353.

2 S. I. Orimo, Y. Nakamori, J. R. Eliseo, A. Zuttel, C. M. Jensen, *Chem. Rev.* 2007, **107**, 4111.

3 B. Bogdanovic, M. Felderhoff, S. Kaskel, A. Pommerin, K. Schlichte, F. Schuth, *Adv. Mater.* 2003, **15**, 1012.

4 W. Grochala, P. P. Edwards, *Chem. Rev.* 2004, **104**, 1283.

5 W. George, M. S. D. Crabtree, V. B. Michelle, *Phys. Today* 2004. **57**, 39.

6 A. Klerke, C. H. Christensen, J. Norskov, T. Vegge, *J. Mater. Chem.* 2008. **18**, 2304.

7 A. Zuttel, S. Rentsch, P. Fischer, P. Wenger, P. Sudan, P. Mauron, C. Emmenegger, *J. Alloys Compd.* 2003, 356, 515; (b) P. Mauron, M. Bielmann, A. Remhof, A. Zuttel, J. H. Shim, Y. W. Cho, *J. Phys. Chem. C* 2010, 114, 16801; (c) P. Mauron, F. Buchter, O. Friedrichs, A. Remhof, M. Bielmann, C. N. Zwicky, A. Zuttel, *J. Phys. Chem. B* 2008, 112, 906.

8 K. Chlopek, C. Frommen, A. Leon, O. Zabara, M. Fichtner, *J. Mater. Chem.* 2007, 17, 3496.

9 H. R. Hoekstra, J. J. Katz, *J. Am. Chem. Soc.* 1949, 71, 2488.

10 Y. Nakamori, K. Miwa, A. Ninomiya, H. W. Li, N. Ohba, S. I. Towata, A. Zuttel, S. I. Orimo, *Phys. Rev. B* 2006, 74, 045126.

11 A. B. Burg, H. I. Schlesinger, *J. Am. Chem. Soc.* 1940, 62, 3425.

12 (a) O. Friedrichs, A. Borgschulte, S. Kato, F. Buchter, R. Gremaud, A. Remhof, A. Zuttel, *Chem. Eur. J.* 2009, 15, 5531. (b) R. B. S. Narashimhan, *Aldrichim. Acta.* 1998, 31, 19.

13 M. B. Gilbert, A. K. Douglas, H. S. Joachim,H. I. Ralph, M. S. Robert III., 2007; available at: http://www.hydrogen.energy.gov/pdfs/review07/stp_24_brown.pdf.

14 (a) J. J. Vajo, S. L. Skeith, F. Mertens, *J. Phys. Chem. B* 2005, 109, 3719; (b) J. J. Vajo, W. Li, P. Liu, *Chem. Comm.* 2010, 46, 6687; (c) J. J. Vajo, F. Mertens, C. C. Ahh, R. C. Bowman, B. Fultz, *J. Phys. Chem. B* 2004, 108, 13977.

15 A. F. Gross, J. J. Vajo, S. L. Van Atta, G. L. Olson, *J. Phys. Chem. C* 2008, 112, 5651.

16 Z. T. Xiong, G. T. Wu, H. J. Hu, P. Chen, *Adv. Mater.* 2004, 16, 1522.

17 (a) F. E. Pinkerton, G. P. Meisner, M. S. Meyer, M. P. Balogh, M. D. Kundrat, *J. Phys. Chem. B* 2005, 109, 6; (b) F. E.; Pinkerton, M. S. Meyer, *J. Alloy. Compd.* 2008, 464, L1; (c) F. E. Pinkerton, M. S. Meyer, G. P. Meisner, *J. Alloy. Compd.* 2007, 433, 282.

18 H. L. Chu, Z. T. Xiong, G. T. Wu, J. P. Guo, T. He, P. Chen, *Dalton. Trans.* 2010, 39, 10585.

19 A. Gutowska, L. Li, Y. Shin, C. M. Wang, X. S. Li, J. C. Linehan, R. S. Smith, B. D. Kay, B. Schmid, W. Shaw, M. Gutowski, T. Autrey, *Angew. Chem. Int. Ed*. 2005, 44, 3578.

20 G. Soloveichik, J. H. Her, P. W. Stephens, Y. Gao, J. Rijssenbeek, M. Andrus, J. Zhao, C. *Inorg. Chem.* 2008, 47, 4290.

21 H. L. Chu, G. T. Wu, Z. T. Xiong, J. P. Guo, T. He, P. Chen, *Chem. Mater*. 2010, 22, , 6021.

22 Y. H. Guo, G. L. Xia, Y. H. Zhu, L. Gao, X. B. Yu, *Chem. Commun.* 2010, 46, 2599.

23 Y. H. Guo, W. W. Sun, Z. P. Guo, H. K. Liu, D. L. Sun, X. B. Yu, *J. Phys. Chem. C* 2010, 114, 12823.

24 (a) Y. H. Guo, X. B. Yu, W. W. Sun, D. L. Sun, W. N. Yang, *Angew. Chem. Int. Ed*. 2011, 50. 1087. (b) Y. H. Guo, H. Wu, W. Zhou, X. B.Yu, *J. Am. Chem. Soc*. 2011, 133, 4690.

25 R. Z. Sørensen, J. S. Hummelshøj, A. Klerke, J. B. Reves, T. Vegge, J. K. Nørskov, C. H. Christensen, *J. Am. Chem. Soc*. 2008, 130, 8660.

26 L. Gao, Y. H. Guo, G. L. Xia, X. B. Yu, *J. Mater. Chem.* 2009, 19, 7826.

27 L. Gao, Y. H. Guo, Q. Li, X. B. Yu, *J. Phys. Chem. C* 2010, 114, 9534.

28 E. Jeon, Y. Cho, *J. Alloys Compd*. 2006, 422, 273.

29 S. Srinivasan, D. Escobar, Y. Goswami, E. Stefanakos, *Int. J. Hydrogen Energy* 2008, 33, 2268.

30 T. Nakagawa, T. Ichikawa, Y. Kojima, H. Fujii, *Mater. Trans.* 2007, 3, 556.

31 A. B. E.Zirngiebl, *W. Ger. Pat*. 1959, 070, 148.

32 T. Yamaguchi, O. Lindqvist, *Acta Chem. Scand*. 1981, 35, 727.

33 K. S. W. B. J. K. D. Wang, *AIP Conf. Proc*. 2007, 879, 879.

34 A. Bergamaschi, A. Cervellino, R. Dinapoli, F. Gozzo, B. Henrich, I. Johnson, P. Kraft A. Mozzanica, B. Schmitt, X. Shi, *J. Synchrot. Radiat*. 2010, 17, 653.

35 S. J. Clark, M. D. Segall, C. J. Pickard, P. J. Hasnip, M. J. Probert, K. Refson, M. C. Payne, *Z. Kristall*. 2005, 220, 567.

36 M. D. Segall, P. J. D. Lindan, M. J. Probert, C. J. Pickard, P. J. Hasnip, S. J. Clark, M. C. Payne, *J. Phys.: Condens Matter* 2002, 14, 2717.

37 J. P. Perdew, K. Burke, M. Ernzerhof, *Phys. Rev. Lett.* 1996, 77, 3865.

38 B. G. Pfrommer, M. Cote, S. G. Louie, M. L. Cohen, *J. Comput. Phys*. 1997, 131, 233.

39 T. J. Marks, J. R. Kolb, *Chem. Rev*. 1977, 77, 263.

40 D. L. A. Boultif, *J. Appl. Crystallogr*. 1991, 24, 987.

41 Favre-Nicolin, V.; Cerny, R. *J. Appl. Cryst.* 2002, 35, 734.

42 Bruker AXS (2008): TOPAS V4.2: General profile and structure analysis software for powder diffraction data. - User's Manual, Bruker AXS, Karlsruhe, Germany.

43 R. D. Shannon, *Acta Crystallogr., Sect. A* 1976, 32, 751.

44 D. Ravnsbaek, Y. Filinchuk, Y. Cerenius, H. J. Jakobsen, F. Besenbacher, J. Skibsted, T. R. Jensen, *Angew. Chem. Int. Ed*. 2009, 48, 6659.

45 G. Wolf, J. Baumann, F. Baitalow, F. P. Hoffmann, *Thermochim. Acta* 2000, 343, 19.

46 A. D. Sutton, A. K. Burrell, D. A. Dixon, E. B. Garner III, J. C. Gordon, T. Nakagawa, K. C. Ott, J. P. Robinson, M. Vasiliu, *Science* 2011, 331, 1426.

47 S. J. Hwang, R. C. Bowman, J. W. Reiter, J. Rijssenbeek, G. L. Soloveichik, J. C. Zhao, H. Kabbour, C. C. Ahn, *J. Phys. Chem. C* 2008, 112, 3164.

48 C. Gervais, J. Maquet, F. Babonneau, C. Duriez, E. Framery, M. Vaultier, P. Florian, D. Massiot, *Chem. Mater*. 2001, 13, 1700.

49 M. K. P. Kohout, F. R. Wagner, Y. Grin, *Theor. Chem. Acc*. 2004, 112, 453.

50 For ELF calculation details please see: http://www.cpfs.mpg.de/ELF.